Numerical methods for a nonlinear reaction-diffusion system modelling a batch culture of biofilm ☆

Eva Balsa-Canto[a], Alejandro López-Núñez[b], Carlos Vázquez[b]

[a] *Process Engineering Group, IIM-CSIC. Spanish Council for Scientific Research. Eduardo Cabello 6, 36208 Vigo, Spain*
[b] *Department of Mathematics, University of A Coruña. Campus Elviña s/n, 15071 – A Coruña (Spain)*

Abstract

A biofilm is usually defined as a layer of bacterial cells anchored to a surface. These cells are embedded into a polymer matrix that keeps them attached to each other and to a solid surface. Among a large variety of biofilms, in this paper we consider *batch* cultures. The mathematical model is formulated in terms of a quasilinear system of diffusion-reaction equations for biomass and nutrients concentrations, which exhibits possible degeneracy and singularities in the nonlinear diffusion coefficient. In the present paper, we propose a set of efficient numerical methods that speeds up the solution of the model. Mainly, Crank-Nicolson finite differences techniques for discretization are combined with a Newton algorithm for the nonlinearities. Moreover, some numerical examples show the expected behaviour of the biomass and nutrients concentrations and also clearly illustrate some theoretically proved qualitative properties related to exponential decays or convergence to a critical biomass concentration depending on the values of the model parameters.

Keywords: Biofilms, continuum models, nonlinear reaction-diffusion equations, numerical methods, Crank-Nicolson

1. Introduction

A biofilm is usually defined as a layer of bacterial cells anchored to a surface. These cells are embedded into a a biological matrix formed mainly by polymers called exopolysaccharides (EPS), that keeps them attached to each other and to a solid surface, thus protecting them and making difficult their removal [14, 15]. In a simplified form, a biofilm can be understood as a group of microorganisms anchored to a surface. Actual studies estimate that less than 0.1 % of all the aquatic microbial life are planktonic microorganisms [1]. Therefore, biofilms are the preferred microbial life form. This preference comes from the fact that the ability to stick to surfaces and form biofilms represents a competitive advantage with respect to a suspended bacteria alternative, because the latter can be easily washed out by water flow, while the former are protected against that phenomena and can grow in an environment with abundance of nutrients. The physical structure of biofilms allows the distinction of biological niches which guarantee the growth and survival of microorganisms that could not compete in a homogeneous system. Additionally, the microbial activity inside biofilms can modify the inner environment in order to make the biofilm more hospitable than the liquid region [12].

The main points to be distinguished in a biofilm are the surface, the biofilm layer, the boundary layer the bulk liquid and the environmental conditions. The surface is where the bacteria are anchored, the biofilm itself is formed by cells of one or various species and the EPS, the boundary layer is optional (as

☆This work has been partially funded by MINECO of Spain (Project MTM2013-47800-C2-1-P).
Email addresses: ebalsa@iim.csic.es (Eva Balsa-Canto), alopeznu@gmail.com (Alejandro López-Núñez), carlosv@udc.es (Carlos Vázquez)

it may exist or not), the bulk liquid is the region where the nutrients are located, and the environmental conditions characterize the biofilm development.

Sometimes biofilms can be beneficial, either for humans or for the natural ecosystem; however sometimes biofilms result to be harmful, thus causing health or economical problems. Sometimes, the former are industrially used on purpose, for example, in water treatment (drip irrigation filters, RBCs, biological reactors, etc.), or they naturally appear underground (contributing to soil or underground water decontamination), in rivers, lakes and coastal zones (where biofilms can be easily seen colonizing rocks), or in plant life's roots. Clearly, the development of natural biofilms is essential for Earth's biosphere. Also bioremediation is currently becoming a higly growing area.

On the other hand, harmful biofilms appear in various situations. For instance, biofilms constitute an important problem in dental hygiene (dental plaque), infectious diseases (legionellosis) or diseases caused by different medical implants (pacemakers, artificial joints or catheters), as well as potable water contamination or the malfunction of heat transfers and heat exchangers. The harmful biofilms formation is an important problem in health industry, where they constitute a mayor source of food contamination (for example, in seafood, poultry or meat processing), with many consequences to consumers.

In general, prevention of harmful biofilm formation is quite hard, because they are capable of growing in very adverse conditions. Also, one must acknowledge the difficulty of biofilm elimination, because the bacteria forming the biofilm are more resilient to the immunological response of the host or to the possible antimicrobial agents.

Either motivated by the need to enhance their beneficial properties or in order to control their evolution, a lot of research has been developed to understand biofilm mechanisms and their modeling. This research tries to investigate the genetic, biochemical and physical mechanisms that contribute not only to the biofilm formation, but also to characterize its structure.

Many studies indicate that the biofilm structure determines the magnitude of the involved inner processes, such as the nutrients transference rate to the lower layers, the microbial agents diffusion rate or the ability to resist frictions. In this sense, various works highlight the microscopic techniques as the most promising for the observation of the developing process of biofilms and their structures. These works, that qualitatively characterize the most basic structures, have given way to others that achieve a quantitative characterization. In that context, two main strategies can be distinguish: mathematical modelling and quantitative image analysis [16]. As we will show later, the present paper can be classified in the first approach.

Among a large variety of biofilms, this paper will focus on *Listeria monocytogenes* strains, a pathogen bacteria associated to food consumption and widely acknowledged by the food safety agencies (AESAN, EFSA), as a high risk bacteria, especially because of its high mortality rate (around 20 %) on pregnant women and immunodeficient people (particular group at risk). The precise motivation comes from the experimental studies and characterization of its biofilm structure, currently being developed at the Institute of Marine Research. For this purpose, *batch* cultures and cellular stain are used, thus allowing to visualize *in vivo* viable biofilm cells by means of a fluorescence microscope. This experimental study analyzes the temporal evolution of the biofilm formation for different strains through the quantitative analysis of the resulting images.

In parallel to these experimental studies, the use of efficient mathematical models allows the prediction of the biofilm evolution for particular values of the involved parameters associated to different conditions. Moreover, it opens the possibility to control and optimize this evolution, in order to satisfy certain objectives. As indicated in [14], the mathematical modeling of biofilms dates back to the 70s of the last century, with very simple initial models mainly focusing on the nutrients flux from the liquid region to the biofilm. Since these seminal models, biofilm modeling has largely evolved and modern models are grouped into cellular automata, discrete and continuous models [9, 10, 11]. The first two ones, specially cellular automata, are mainly based on local probability rules. Although their results highly agree with experiments, many physical issues remain actually unclear. For example, the results strongly depend on the discretization, with significant qualitative and quantitative differences. Alternatively, continuum models usually consider the biofilm as a material, for example, as a viscous fluid. More precisely, a two-phase fluid can be considered, thus separating the fluid containing nutrients and the

one containing biomass. In the continuous setting, the involved physical magnitudes usually are the solution of complex systems of nonlinear partial differential equations of convection-diffusion-reaction type. Due to their complexity, the analytical expression of these solutions are not available, so that efficient numerical methods to get enough accurate approximations are required.

Having in view the different characteristics of the particular biofilm, in the present paper we consider a continuum model. These main characteristics are: the number of cells in the batch culture is very high (greater than 10^5), so that the cellular growth is extremely slow, non motile cells are considered, and the cellular dispersion appears when a certain threshold of the cellular density is achieved. Taking into account the previous conditions, in order to describe biofilm formation of *L. monocytogenes* we consider the continuum model proposed in [4]. This model is posed in terms of a system of nonlinear time dependent reaction-diffusion equations, with suitable boundary conditions depending on the particular regimes to be considered for the biofilm. Possible degeneracy and singularities in the biomass equation are the main difficulties from the theoretical and numerical point of views. In [4], the numerical solution is mainly based on first order time discretization schemes, combined with a central finite difference scheme in space. More precisely, the conditional stability of explicit scheme requires a smaller time step and is used for the biomass equation, while the nutrient transport is solved with the implicit scheme. More recently, in [2] a transformation of unknown is applied to the biomass equation, so that the nonlinearity is shifted to the term of time derivative, while the diffusion part is linearized and writen in terms of a Laplace operator. Next, an implicit Euler scheme leads to a nonlinear elliptic problem at each time step, which is discretized by piecewise linear finite elements combined with a SOR-Newton method for the fully discretized problem. A rigorous numerical analysis is developed and the examples mainly correspond to academic cases to illustrate the performance of the method. Although, it overcomes very well the singularity, spurious oscillations may appear which are related to the degeneracy aspect. In [3], an explicit in time treatment of the diffusion coefficient combined with a low order non-standard finite differences in time for the biomass equation is proposed, thus leading to constraints on the size of the local time step for the stability of the proposed finite differences scheme. However, the method does not exhibit oscillations and is positivity preserving.

In order to avoid the constraints on the time step size in the literature and to increase the order of convergence in time, we propose a second order Crank-Nicolson time discretization scheme. In this way, larger time steps are allowed for the discretization in time of the system and the computational cost to obtain accurate approximations of the biomass and nutrient concentrations at final time can be highly reduced. Additionally, the numerical solutions do not exhibit oscillations and preserve the positivity property in the whole computational domain.

The present model can be framed in the one mathematically analyzed in [5], where the existence, uniqueness and qualitative properties of the solution are obtained. The numerical results in the different examples are in agreement with this theoretical analysis. In particular, under certain conditions in the coefficients of the equations, a theoretically proved exponential decay of the biomass is illustrated by the numerical experiments.

The plan of the paper is as follows. In Section 2 the mathematical model is posed. In section 3 the different numerical methods are fully described. In Section 4, a set of numerical examples illustrates the performance of the numerical methods as well as the qualitative and quantitative behaviour of the involved magnitudes in the continuous model.

2. Mathematical Model

2.1. Model description

As indicated in the previous section, we mainly follow the model described in [4], with some extra simplifications in accordance to the experiments being carried out at the IIM-CSIC with *L. monocytogenes* biofilm. Among the required properties to be fulfilled are the following:

i. Existence of a "sharp front" of biomass at the transition from fluid to solid

ii. Biomass spreading is more relevant when a certain density is achieved
iii. Biomass density cannot exceed a certain maximum
iv. Biomass productions is caused by a reaction process
v. The spreading mechanism must be compatible with the nutrients consumption and transference model. Also, we are working in a *batch* system, so that the hydrodynamic effects are neglected
vi. Given the biochemical parameters, the spatial heterogeneities in a biofilm come from environmental conditions

The biomass bound stated in *iii)* cannot be due to the reaction terms (*iv)*. It must be associated to the biomass spreading process. Moreover, that bound can be a consequence of *ii)*. Additionally, the propagation mechanism will be a diffusive flux, that can not be associated to a constant diffusion coefficient, because in that case there would be an instantaneous diffusion, thus contradicting *ii)* and not guaranteeing neither the biomass limit nor the fulfilment of *i)*. Therefore, a diffusion coefficient depending on the biomass density and vanishing in the liquid region is required. The environmental conditions responsible for the nutrients availability are taken into account by means of a good description of the transport processes in the liquid region, namely the hydrodynamics and mass transference processes.

In order to pose a evolutive model in a one-dimensional spatial domain, we consider $\Omega = (0, L)$, in which we distinguish two time dependent regions: $\Omega_1(t)$, which represents the liquid bulk, and $\Omega_2(t)$, which represents the part occupied by the biomass. Both regions can be characterized by the value of the biomass density, m: $m(t, x) = 0$ for all points x in $\Omega_1(t)$ and $m(t, x) > 0$ for any x in $\Omega_2(t)$. Thus, the main unknowns of the model are the biomass density, m, and the nutrients concentration, c, both defined on $(0, T) \times \Omega$, and satisfying the following system of nonlinear partial differential equations

$$\frac{\partial c}{\partial t} + u \cdot \nabla c = \nabla \cdot (d_1(m)\nabla c) - f(c, m) \quad \text{in } (0, T) \times \Omega, \tag{1}$$

$$\frac{\partial m}{\partial t} = \nabla \cdot (d_2(m)\nabla m) + g(c, m) \quad \text{in } (0, T) \times \Omega, \tag{2}$$

where d_1 and d_2 denote the diffusion coefficients for the nutrients and biomass, respectively; both depending on m. Moreover, functions f and g are associated to the nutrients consumption and biomass production rates, respectively, and are given by

$$f(c, m) = \frac{k_1 c m}{k_2 + c}, \quad g(c, m) = k_3(f(c, m) - k_4 m), \tag{3}$$

where the involved constants k_i are provided in a forthcoming table. The problem formulation is completed by appropriate boundary and initial conditions which depend on the operating regime of the biofilm.

The function u represents the velocity field of the fluid in the liquid region, which is obtained from the solution of the incompressible Navier-Stokes equation in this region. However, as we will consider a batch biofilm, the first simplification consists of taking $u = 0$.

Note that Equation (1) describes the transport of nutrients, which is convective and diffusive in Ω_1 while is only diffusive in Ω_2. Equation (1) has been widely studied, while equation (2) was first proposed in [4] as a biomass density evolution equation. Biomass spreading is given by the diffusive flux $d_2(m)\nabla m$. The formation of new biomass is given by $g(c, m)$, described in (3), which includes a wasting term $-k_3 k_4 m$. As $g(c, m)$ is the only biomass source, the fulfillment of *iv)* is guaranteed. The property *v)* is satisfied by (1), provided that a sharp front separating Ω_1 and Ω_2 is obtained, as stated in *i)*.

The parameters k_i, $i = 1, \ldots, 4$, are non negative and characterized by the particular problem taken in account. We assume that $d_1(m)$ is positive, bounded and piece-wise differentiable. The biomass diffusion function $d_2(m)$ must be so that properties *i)-vi)* are satisfied. So, as indicated in [8], $d_2(m)$ takes the following form:

$$d_2(m) = \left(\frac{\epsilon}{m_{max} - m}\right)^a m^b, \tag{4}$$

where m_{max} represents the upper limit postulated by *iii)*.

Note that function d_2, defined by (4), is zero as long as $m = 0$ and near zero when m is much more smaller than m_{max}. While m is near m_{max}, $d_2(m)$ becomes very large and produces a non negligible diffusive transport. The parameter a must be so that *iii)* is guaranteed, while ϵ and b must guarantee the conditions *i)* and *ii)*.

2.2. Model simplifications and dimensionless equations

First, according to the statement in property *v)*, we assume a *batch* flux, thus taking $u = 0$ and avoiding the need of solving Navier-Stokes equations to characterize the hydrodynamics as in a more general model.

Secondly, as the nutrients diffusivity at the biofilm and the liquid region are usually of the same order of magnitude, and taking into account that our work mainly focuses on the biomass evolution, we will assume that d_1 is constant.

Moreover, in order to pose the problem in dimensionless form, we consider the dimensionless variables $M := m/m_{max}$ and $C := c/c_0$, so that the simplified equivalent dimensionless model can be written as:

$$\frac{\partial C}{\partial t} = d_1 \nabla^2 C - F(C, M) \tag{5}$$

$$\frac{\partial M}{\partial t} = \nabla \cdot (d_2(M) \nabla M) + G(C, M), \tag{6}$$

where

$$F(C, M) = K_1 \frac{MC}{K_2 + C} \tag{7}$$

$$G(C, M) = K_3 \frac{CM}{K_2 + C} - K_4 M \tag{8}$$

$$d_2(M) = m_{max}^{b-a} \left(\frac{\epsilon}{1 - M} \right)^a M^b \tag{9}$$

We are considering the 1D version of equations (5) and (6), so that we assume that functions C and M satisfy the following system of PDEs in the domain $(0, T) \times (0, L)$:

$$C_t = d_1 C_{xx} - F(C, M) \tag{10}$$

$$M_t = (d_2(M) M_x)_x + G(C, M), \tag{11}$$

The parameters K_i appearing in (5)-(6) are

$$K_1 = m_{max} \frac{k_1}{c_0}, \quad K_2 = \frac{k_2}{c_0}, \quad K_3 = k_3 k_1, \quad K_4 = k_3 k_4,$$

which in turn depend on

$$k_1 = m_{max} \left(\frac{\mu_m}{Y_{XS}} + m_s \right), \quad k_2 = K_s, \quad k_3 = Y_{XS}/m_{max}, \quad k_4 = m_s m_{max},$$

where the remaining parameters are described in Table 1.

3. Numerical Methods

As it is not possible to obtain analytically the solution of the system of nonlinear partial differential equations (5)-(6), appropriate numerical methods are required to efficiently compute the approximation

of the solution. In the previous work [4], a combination of explicit and implicit finite difference methods have been used. More precisely, a explicit time-stepping has been used in (6) while a fully implicit scheme has been applied to (5). Note that the explicit scheme involves a stability constraint on the time step, thus limiting the use of large time steps. In both equations, a classical centered scheme is used in the spatial discretization. The resulting nonlinear system associated to the fully discretized problem is solved with a Newton-BiCGSTAB method. The main drawback of this numerical strategy comes from the use of an explicit scheme that requires a large number of time steps to obtain the concentration of nutrients and biomass at final time, thus leading to an extremely slow algorithm. Additionally, it should be noticed that the finite-differences scheme is first order in time.

More recently, in [17] the fully implicit scheme has been applied in combination with a Newton algorithm for the nonlinear fully discretized problem. Although with this alternative approach the stability constraint is not present, in order to properly approximate these slow nonlinear diffusion processes small time steps are required and the fully implicit feature also leads to very large computational times.

In the present paper, we propose the use of Crank-Nicolson finite difference scheme, which is second order in time and space [7], so that larger time steps can be used for the same accuracy and thus reduce the computational time. For this purpose, we first consider a finite differences mesh, with a number of time intervals, N, and a number of spatial nodes, J, in terms of which we define the time and spatial steps, respectively, as

$$\Delta t = \frac{T}{N}, \quad \Delta x = \frac{L}{J-1}$$

and lets introduce the notation for the approximations of the solution, $C_j^n \approx C(n\Delta t, j\Delta x)$ and $M_j^n \approx M(n\Delta t, j\Delta x)$, with $n = 0, \ldots, N$ and $j = 0, \ldots, J-1$.

Equations (10) and (11) are discretized with a Crank-Nicolson finite differences in time and central differences for the second order derivative in space. Applying the method first to equation (10), for $n = 0,\ 1 \ldots, N-1$, we obtain the system of equations

$$\begin{aligned}\frac{C_j^{n+1} - C_j^n}{\Delta t} &= \frac{1}{2}\left[d_1 \frac{(C_{j+1}^n - 2C_j^n + C_{j-1}^n)}{(\Delta x)^2} - F(C_j^n, M_j^n)\right] + \\ &\quad \frac{1}{2}\left[d_1 \frac{(C_{j+1}^{n+1} - 2C_j^{n+1} + C_{j-1}^{n+1})}{(\Delta x)^2} - F(C_j^{n+1}, M_j^{n+1})\right],\end{aligned}$$

for $j = 1, \ldots, J-1$. Next, reordering the terms, we get

$$\begin{aligned}C_j^{n+1} - C_j^n &= \frac{d_1\Delta t}{2(\Delta x)^2}(C_{j+1}^n - 2C_j^n + C_{j-1}^n) - \frac{\Delta t K_1 C_j^n M_j^n}{2(K_2 + C_j^n)} + \frac{d_1\Delta t}{2(\Delta x)^2}(C_{j+1}^{n+1} - 2C_j^{n+1} + C_{j-1}^{n+1}) \\ &\quad - \frac{\Delta t K_1 C_j^{n+1} M_j^{n+1}}{2(K_2 + C_j^{n+1})},\end{aligned}$$

or equivalently, we have

$$-\omega C_{j+1}^{n+1} + (1+2\omega)C_j^{n+1} - \omega C_{j-1}^{n+1} + \sigma\frac{C_j^{n+1}M_j^{n+1}}{K_2 + C_j^{n+1}} + \left[-\omega C_{j+1}^n + (2\omega - 1)C_j^n - \omega C_{j-1}^n + \sigma\frac{C_j^n M_j^n}{K_2 + C_j^n}\right] = 0, \quad (12)$$

where $\omega = \dfrac{d_1\Delta t}{2(\Delta x)^2}$ and $\sigma = \dfrac{\Delta t K_1}{2}$.

Next, applying a central scheme to approximate the most external spatial derivatives in equation (11), we get

$$\begin{aligned}\frac{M_j^{n+1} - M_j^n}{\Delta t} &= \frac{1}{2}\left[\frac{d_2(M_{j+1}^n)(M_{j+1}^n)_x - d_2(M_{j-1}^n)(M_{j-1}^n)_x}{2\Delta x} + G(C_j^n, M_j^n)\right] \\ &\quad + \frac{1}{2}\left[\frac{d_2(M_{j+1}^{n+1})(M_{j+1}^{n+1})_x - d_2(M_{j-1}^{n+1})(M_{j-1}^{n+1})_x}{2\Delta x} + G(C_j^{n+1}, M_j^{n+1})\right].\end{aligned}$$

As d_2 is positive, we use a backward scheme in space in the remaining spatial derivatives in previous equations, thus obtaining

$$\begin{aligned}\frac{M_j^{n+1}-M_j^n}{\Delta t} &= \frac{1}{2}\left[\frac{d_2(M_{j+1}^n)(M_{j+1}^n-M_j^n)-d_2(M_{j-1}^n)(M_j^n-M_{j-1}^n)}{2\Delta x}+G(C_j^n,M_j^n)\right]\\ &+\frac{1}{2}\left[\frac{d_2(M_{j+1}^{n+1})(M_{j+1}^{n+1}-M_j^{n+1})-d_2(M_{j-1}^{n+1})(M_j^{n+1}-M_{j-1}^{n+1})}{2\Delta x}+G(C_j^{n+1},M_j^{n+1})\right].\end{aligned}$$

Furthermore, applying the definition of d_2, we have

$$\begin{aligned}M_j^{n+1}-M_j^n &= \frac{\Delta t m_{max}^{b-a}\epsilon^a}{4(\Delta x)^2}\left[\frac{(M_{j+1}^n)^{b+1}-(M_{j+1}^n)^bM_j^n}{(1-M_{j+1}^n)^a}-\frac{(M_{j-1}^n)^bM_j^n-(M_{j-1}^n)^{b+1}}{(1-M_{j-1}^n)}\right]\\ &+\frac{\Delta t m_{max}^{b-a}\epsilon^a}{4(\Delta x)^2}\left[\frac{(M_{j+1}^{n+1})^{b+1}-(M_{j+1}^{n+1})^bM_j^{n+1}}{(1-M_{j+1}^{n+1})^a}-\frac{(M_{j-1}^{n+1})^bM_j^{n+1}-(M_{j-1}^{n+1})^{b+1}}{(1-M_{j-1}^{n+1})}\right]\\ &+\frac{\Delta t}{2}G(C_j^n,M_j^n)+\frac{\Delta t}{2}G(C_j^{n+1},M_j^{n+1}).\end{aligned}$$

Finally, by introducing the definition of G and rearranging terms, we have

$$\begin{aligned}&\left(1+\frac{\Delta tK_4}{2}\right)M_j^{n+1}+\mu\left[\frac{(M_{j+1}^{n+1})^bM_j^{n+1}-(M_{j+1}^{n+1})^{b+1}}{(1-M_{j+1}^{n+1})^a}+\frac{(M_{j-1}^{n+1})^bM_j^{n+1}-(M_{j-1}^{n+1})^{b+1}}{(1-M_{j-1}^{n+1})}\right]\\ &+\left(\frac{\Delta tK_4}{2}-1\right)M_j^n+\mu\left[\frac{(M_{j+1}^n)^bM_j^n-(M_{j+1}^n)^{b+1}}{(1-M_{j+1}^n)^a}+\frac{(M_{j-1}^n)^bM_j^n-(M_{j-1}^n)^{b+1}}{(1-M_{j-1}^n)}\right]\\ &-\frac{\Delta tK_3}{2}\frac{C_j^{n+1}M_j^{n+1}}{K_2+C_j^{n+1}}-\frac{\Delta tK_3}{2}\frac{C_j^nM_j^n}{K_2+C_j^n}=0.\end{aligned}$$

Once the boundary conditions are taken into account, we obtain a system of nonlinear equations we write in the form

$$\mathcal{F}(\mathbb{X}^{n+1}) = 0, \tag{13}$$

where the definition of $\mathcal{F}$ depends on the particular boundary conditions. Different boundary conditions are considered in the forthcoming test examples. The unknown vector $\mathbb{X}^{n+1}$ in (13) contains the components of the vectors $C^{n+1}=(C_j^{n+1})_{j=0}^{J-1}$ and $M^{n+1}=(M_j^{n+1})_{j=0}^{J-1}$, which are ordered so that the resultant system is as simpler as possible.

As the function $\mathcal{F}$ is nonlinear, in order to solve (13) we propose the use of the Newton method [6]. Thus, starting from $\mathbb{Y}^0=\mathbb{X}^n$, at the iteration p we compute $\mathbb{Y}^{p+1}$ as follows:

$$J_{\mathcal{F}}(\mathbb{Y}^p)\Delta\mathbb{Y}^p = \mathcal{F}(\mathbb{Y}^p) \tag{14}$$

$$\mathbb{Y}^{p+1} = \mathbb{Y}^p-\Delta\mathbb{Y}^p, \tag{15}$$

where $J_{\mathcal{F}}(\mathbb{Y})$ denotes the Jacobian matrix of $\mathcal{F}$ at the point $\mathbb{Y}$. At each Newton iteration, the solution of the linear system (14), $\Delta\mathbb{Y}^p$, is obtained from an optimized pentadiagonal LU factorization (analogous to Thomas algorithm for tridiagonal matrices). Finally, we find $\mathbb{X}^{n+1}$ through the calculation of the sequence $\mathbb{Y}^p$, until achieving an index so that the required relative error tolerance between two consecutive iterations is fulfilled. That index will provide the value of $\mathbb{X}^{n+1}$.

4. Numerical Results

In order to validate the performance of the set of numerical methods and compare it with the alternative explicit and fully implicit techniques previously proposed in the literature, we consider some numerical

examples first presented in [4]. In all examples in this section, the problem is formulated in terms of the system of PDEs (10)-(11), where the involved function coefficients are given by expressions (7), (8) and (9). Table 1 shows a brief description and units of all the parameters and their values when they are common for all cases, while Table 2 shows the specific parameter values of K_s, m_{max} and c_0 for particular cases.

It is important to point out that the following four cases can be framed inside the general system of equations with pure Neumann boundary conditions for the biomass that has been mathematically analyzed in [5], where the existence, uniqueness and some qualitative properties of the solution are obtained. In particular, it is proved that if the condition

$$K_3/(1+K_4) - K_2 \leq 0 \tag{16}$$

holds, then the biomass concentration decays exponentially with respect to time. Moreover, under condition (16), the solution exists globally in time for any initial concentrations of nutrients and biomass. However, when condition (16) is not fulfilled, then there exist initial data such that the biomass concentration reaches the value 1 for at a critical time T_0, so that the corresponding diffusion coefficient in the biomass equation blows up (as illustrated in the forthcoming Case E presented in Section 4.5).

In Table 3 we show the constant value of the left hand in (16) for the chosen parameters in all forthcoming examples, so that inequality (16) is satisfied and consequently a global solution exists and a exponential decay in biomass is expected. Note the the numerical results presented in this section are in full agreement with this theoretically proved property.

The numerical results for all forthcoming cases in this Section have been obtained with the proposed Crank-Nicolson discretization scheme. All of them are in agreement with those ones previously obtained from alternative combinations of explicit and implicit schemes or fully implicit ones in [4, 17]. The main advantage of using the second order in time scheme of Crack-Nicolson is the division by around three times the computational time to achieve the magnitude values at final time T, as larger time steps (and therefore, less time iterations) can be used to obtain the same kind of results.

Concerning the discretization parameters, in all examples the values $\Delta t = 1.44 \times 10^{-4}$ seconds and $\Delta x = 1.5873 \times 10^{-6}$ meters for the time and spatial steps, respectively, have been taken. They correspond to $N = 5 \times 10^9$ time iterations to achieve $T = 200$ and $J = 64$ mesh nodes in space, respectively. Moreover, the tolerance value 10^8 for the convergence in the Newton method has been taken.

4.1. Case A: Solid surface growth

In the first case we are initially considering a bacterial inoculum attached to the solid wall at $x = 0$, with thickness of 3.2×10^{-6}m, while we place a fixed nutrients concentration at $x = L$. Therefore, the following boundary and initial conditions for the nutrients are considered:

$$C_x(t,0) = 0, \quad t \in [0,T], \tag{17}$$
$$C(t,L) = 1, \quad t \in [0,T], \tag{18}$$
$$C(0,x) = 1, \quad x \in [0,L], \tag{19}$$

while the following ones are taken for the biomass concentration:

$$M_x(t,0) = 0, \quad t \in [0,T], \tag{20}$$
$$M_x(t,L) = 0, \quad t \in [0,T], \tag{21}$$
$$M(0,x) = \begin{cases} M_0, & \text{if } 0 \leq x \leq 3.2 \times 10^{-6}, \\ 0, & \text{if } 3.2 \times 10^{-6} < x \leq L. \end{cases} \tag{22}$$

Previously considered boundary and initial conditions aim to show the biomass evolution when initially a colony is attached to a solid surface and can only expand to one side. The resulting evolution can be observed in Figures 1 and 2, in which additionally the expected front with sharp gradient is shown. This front separates the liquid from the solid regions as postulated in *i)*. Moreover, the dispersion mechanism

causes the initial large dispersion to adjacent cells from those ones having a positive initial biomass concentration. Next, once the biomass concentration decreases, such diffusion phenomenon is reduced. As the biomass concentration is nonuniform at $t = 0$, the initially uniform nutrients concentration is instantaneously destroyed and becomes non uniform immediately after the initial time. Note also as the nutrients concentration at $x = 0$ tends rapidly to zero.

4.2. Case B: One-dimensional growth with asymmetric boundary conditions

In this case we illustrate the influence of the involved environmental and biological parameters on the biomass growth and dispersion. For this purpose, we consider an initial biomass concentration located in a small interval of width 3.2×10^{-6} at the center of the computational domain $[0, L]$, while the nutrients enter the system through the boundary $x = L$. In addition, three subcases are be considered in this case, which correspond to three different sets of the parameters m_{max} and c_0, as indicated in Table 2.

Therefore, the following boundary and conditions have been considered for the nutrients concentration:

$$C_x(t,0) = 0, \quad t \in [0,T], \tag{23}$$
$$C(t,L) = 1, \quad t \in [0,T], \tag{24}$$
$$C(0,x) = 1, \quad x \in [0,L], \tag{25}$$

while for the biomass we impose the following ones:

$$M_x(t,0) = 0, \quad t \in [0,T], \tag{26}$$
$$M_x(t,L) = 0, \quad t \in [0,T], \tag{27}$$
$$M(0,x) = \begin{cases} M_0, & \text{if } x \in [\frac{L}{2} - 1.6 \times 10^{-6}, \frac{L}{2} + 1.6 \times 10^{-6}], \\ 0, & \text{otherwise.} \end{cases} \tag{28}$$

Unlike to the previous case A, now we try to illustrate a situation where biomass propagation takes place both to the left and to the right of the initial biomass region. As the nutrients concentration is nonuniform, a larger growth is expected to be held in the region closer to the location of nutrients source. Note that this behaviour is observed in Figures 3 to 5. Cases B-(b) and B-(c) aim to illustrate how the biomass dispersion is accelerated when decreasing parameter m_{max} (case B-(b), with the corresponding Figure 5), or increasing c_0 (case B-(c), Figure 5). The results for case B-(a) are shown Figure 3 and conclude that the diffusion mechanism is too strong so that there is no much difference at both sides of the initial colony, unlike the other two cases. Particularly, this difference is observed in case B-(b), in which the presence of a larger concentration of nutrients at one side leads to a more slow decay of biomass concentration, thus maintaining larger values of it at this side in comparison with adjacent nodes. Additionally, in case B-(c), the strong diffusion phenomenon combined with a larger formation due to the particular choice of parameters causes an anomalous increase of biomass, although the trend to disappear is common with all the cases exhibited in this Section.

4.3. Case C: One-dimensional growth with symmetric boundary and initial conditions

In order to evaluate the development of the biofilm structure in a regular nutrients field, in this case we consider symmetric boundary conditions. As in the other cases, the specific parameters are listed in Table 2. The specific boundary and initial conditions for the nutrients concentration are the following:

$$C(t,0) = 1, \quad t \in [0,T], \tag{29}$$
$$C(t,L) = 1, \quad t \in [0,T], \tag{30}$$
$$C(0,x) = 1, \quad x \in [0,L], \tag{31}$$

while for the biomass concentration we consider

$$M_x(t,0) = 0, \quad t \in [0,T], \tag{32}$$
$$M_x(t,L) = 0, \quad t \in [0,T], \tag{33}$$
$$M(0,x) = \begin{cases} M_0, & \text{if } x \in [\frac{L-1.6\times10^{-6}}{2}, \frac{L+1.6\times10^{-6}}{2}], \\ 0, & \text{otherwise.} \end{cases} \tag{34}$$

In case C, the presence of a large enough nutrients concentration at both ends of the spatial domain allows for the biofilm growth exhibiting a symmetric concentration distribution, as shown in Figures 7 and 8. As expected, the nutrients concentration is also symmetric, being naturally smaller in regions with larger biomass concentration.

4.4. Case D: One-dimensional growth with two colonies merging under symmetric initial and boundary conditions

Case D illustrates the merging of two biomass fronts. For this purpose, we initially place in the spatial domain two separated colonies of the same size. Additionally, we consider the same boundary conditions as in the previous case C. We will also distinguish two subcases inside case D with two different set of parameters, so that the influence of the involved parameters can be analyzed.

Thus, in case D the following boundary and initial conditions have been take for the nutrients concentration:

$$C(t,0) = 1, \quad t \in [0,T], \tag{35}$$
$$C(t,L) = 1, \quad t \in [0,T], \tag{36}$$
$$C(0,x) = 1, \quad x \in [0,L], \tag{37}$$

while the following ones for the biomass have been taken

$$M_x(t,0) = 0, \quad t \in [0,T], \tag{38}$$
$$M_x(t,L) = 0, \quad t \in [0,T], \tag{39}$$
$$M(0,x) = \begin{cases} M_0, & \text{if } x \in [x_1,x_2] \cup [x_3,x_4], \\ 0, & \text{otherwise,} \end{cases} \tag{40}$$

where

$$x_1 = L - x_4, \quad x_2 = L - x_3, \quad x_3 = L/2 + 3 \times 1.6 \times 10^{-6}, \quad x_4 = L/2 + 4 \times 1.6 \times 10^{-6}.$$

Thus, after the numerical solution with the proposed techniques, Figures 9-11 corresponding to case D illustrate the slow merging of the two colonies. According to the change in the value of M_0, the initial diffusion is smaller so that the the merging process of the colonies slows down. Case D-(b) is designed such that, according to the chosen parameters indicated in Table 2, the merging of the two colonies is delayed (as shown in Figure 10). However, despite of being more slow than in previous examples, diffusion is large enough to not observe any significative differences between cases D-(a) and D-(b) just by comparing Figures 9 and 10. This is the reason why we add Figure 12, in which we present the difference between biomass concentrations obtained in cases D-(a) and D-(b). Note that this difference is positive and of order 10^{-3} thus implying (as expected) that the biomass concentration is larger in case D-(a).

4.5. Case E: Solid surface growth with parameters leading to blow up of solution

In this case, we consider again as in case A the bacterial inoculum attached to the solid wall $x = 0$. However, we modify some parameters, as indicated in Table 2, so that the condition

$$\frac{K_3}{1+K_4} - K_2 > 0$$

is satisfied. Under the previous condition, in [5] it is proved that the solution quenches in finite time, i.e. there exists a finite time T_0, such that

$$M(t,\cdot) < 1, \quad \text{for} \quad t < T_0, \quad \lim_{t \to T_0} M(t,\cdot) = 1.$$

More precisely, the new set of parameters is mainly obtained by significantly reducing K_s from its value in Case A to both cases E-(a) and E-(b). In case E-(a) the value of c_0 is increased with respect to Case A, while in E-(b) we maintain the same value of c_0 as in case A. In Figures 13 and 14 it is illustrated how the biomass tends to one when a certain time is achieved. After that time biomass concentration blows-up. For Case E-(a), the biomass for different times is also illustrated in Figure 15. The same behaviour has been observed in Case E-(b).

5. Conclusions

In this paper a new set of efficient numerical methods for a nonlinear system of reaction-diffusion equations governing the nutrients and biomass concentrations in a biofilm has been proposed. Besides the nonlinearities associated to production and consumption terms, the PDE model presents nonlinear diffusion coefficients that may become degenerate or exhibit singularities when a certain value of biomass concentration is achieved. In order to overcome all difficulties in the numerical solution, an implicit Crank-Nicolson scheme for time discretization is combined with a Newton method for the resulting discretized problem. The choice of the second order Crank-Nicolson scheme allows the use of larger time steps when compared with the fully implicit or the conditionally stable explicit schemes, thus highly reducing the computational time. In order to illustrate the performance of the proposed numerical techniques, several test examples have been chosen. Examples of Cases A to D are taken from [4] and the same kind of results are observed. Moreover, in accordance with the theoretical results in [5], in these cases the expected exponential decay of biomass is observed for the chosen set of parameters. Also we added Case E, in which the set of parameters leads to situations where the initial biomass concentration increases until reaching the value one at a certain critical time, thus achieving a singularity in the nonlinear diffusion coefficient so that a quenching phenomenon arises. The theoretical analysis in [5] proves that this occurs when a constant depending on certain physical parameters becomes positive and the numerical results concerning to Case E clearly show this phenomenon for small positive values of this constant.

References

[1] Costerton J W, Lewandowski Z, Caldwell D E, Korber D R, Lappin-Scott H M. Microbial biofilms. *Annual Review Microbiology*, 49 (1995), 711-745.

[2] Duvnjak A, Eberl H J. Time-discretization of a degenerate reaction-diffusion equations arising in biofilm engineering. *Electronic Transactions on Numerical Analysis*, 23 (2006), 15-37

[3] Eberl H J, Demaret L. A finite difference scheme for a degenerated diffusion equation arising in microbial ecology, *Sixth Mississippi State Conference on Differential Equations and Computational Simulations, Electronic Journal of Differential Equations.*, Conference 15 (2007), pp. 77-95.

[4] Eberl H J, Parker D F, van Loosdrecht M C M. A New Deterministic Spatio-Temporal Continuum Model for Biofilm Development. *Journal of Theoretical Medicine*, 3 (2001), 161-175.

[5] Efendiev M A, Eberl H J, and Zelik S V. Existence and longtime behavior of solutions of a nonlinear reaction-diffusion system arising in the modeling of biofilms. *Nonlinear Diffusive Systems and Related Topics*, 1258 (2002), 49-71.

[6] Epperson J F. *An introduction to numerical methods and analysis*, John Wiley & Sons, 2007.

[7] LeVeque R J , *Finite Difference Methods for Ordinary and Partial Differential Equations: Steady-State and Time-Dependent Problems*. SIAM, 2007.

[8] Murray J D. *Mathematical Biology*. Springer, 1993.

[9] Picioreanu C, van Loosdrecht M C M, Heijnen J J. A new combined differential-discrete cellular automaton approach for biofilm modelling: application for growth in gel beads. *Biotechnology and Bioengineering*, 57 (1998), 718-731.

[10] Picioreanu C, van Loosdrecht M C M, Heijnen J J. Mathematical modelling of biofilm structure with a hybrid differential-discrete cellular automaton approach. *Biotechnology and Bioengineering*, 58 (1998), 101-116.

[11] Picioreanu C, van Loosdrecht M C M. Use of mathematical modelling ato study biofilm development and morphology. In: Lens, P. and others (editors) *Biofilms in Medicine, Industry and Environmental Technology. Characteristics, Analysis and Control*, IWA Publishing (2003), 413-437.

[12] Rittmann B E, McCarty P L. *Environmental Biotechnology. Principles and Applications*, McGraw Hill, 2001

[13] Van Loosdrecht M C M, Picioreanu C, Heijnen J J. A more unifying hypothesis for biofilm structures. *FEMS Microbiology Ecology*, 24 (1997), 181-183.

[14] Wanner O, Eberl H J, Morgenroth E, Noguera D R, Picioreanu C, Rittmann B E, van Loosdrecht M C M. *Mathematical Modelling of Biofilms*. IWA Task Group on Biofilm Modelling, 2006.

[15] Wilderer P A, Characklis W G. *Structure and function of biofilms*. John Wiley & Sons, 1989.

[16] Yang X, Beyenal H, Harking G, Lewandowski Z. Quantifying biofilm structure using image analysis. *Journal of Microbiological Methods*, 39 (2000), 109-119.

[17] López-Núñez A., Mathematical modelling in biofilms (in Spanish). *Master Thesis*, University of A Coruna, 2013.

Parameter	**Brief description (units)**	**Value**
d_1	Nutrients diffusion coefficient (m^2/s)	1.6×10^{-9}
μ_m	Specific growth rate $(1/s)$	1.5×10^{-5}
Y_{XS}	Substrate growth yield factor (*dimensionless.*)	4.5×10^{-2}
K_s	Monod saturation constant (kg/m^3)	Variable
m_s	Maintenance coefficient $(1/s)$	3×10^{-5}
m_{max}	Maximum biomass (kg/m^3)	Variable
c_0	Initial nutrients concentration (kg/m^3)	Variable
M_0	Initial biomass concentration (*dimensionless*)	9×10^{-1}
ϵ	Equation control parameter (*dimensionless*)	5×10^{-5}
a	Biomass dispersion parameter (*dimensionless.*)	4
b	Biomass dispersion parameter (*dimensionless.*)	4
L	Upper bound of the spatial domain $(0, L)$ (m)	1×10^{-4}
T	Final time (h)	200

Table 1: Parameters of the problem: brief description and values in all examples(when fixed).

Param.	A	B-(a)/B-(b)/B-(c)	C	D-(a)/D-(b)	E-(a)/E-(b)
K_s	3.5×10^{-5}	3.5×10^{-5}	3.5×10^{-5}	3.5×10^{-5}	$3.5\times10^{-7}/3.5\times10^{-8}$
m_{max}	60	80/40/40	60	60/90	60
c_0	4×10^{-3}	$2\times10^{-3}/2\times10^{-3}/4\times10^{-3}$	2×10^{-3}	$1\times10^{-3}/2\times10^{-3}$	$4\times10^{-2}/4\times10^{-3}$

Table 2: Values of K_s, m_{max} and c_0 for the different cases in the numerical examples

Coefficient in (16)	A	B-(a)/B-(b)/B-(c)	C	D-(a)/D-(b)	E-(a)/E-(b)
$K_3/(1+K_4)-K_2$	-0.0087	-0.0175/-0.0175/-0.0087	-0.0175	-0.0350/-0.0175	7.5×10^{-6}

Table 3: Values related to the Efendiev condition (16) in different cases

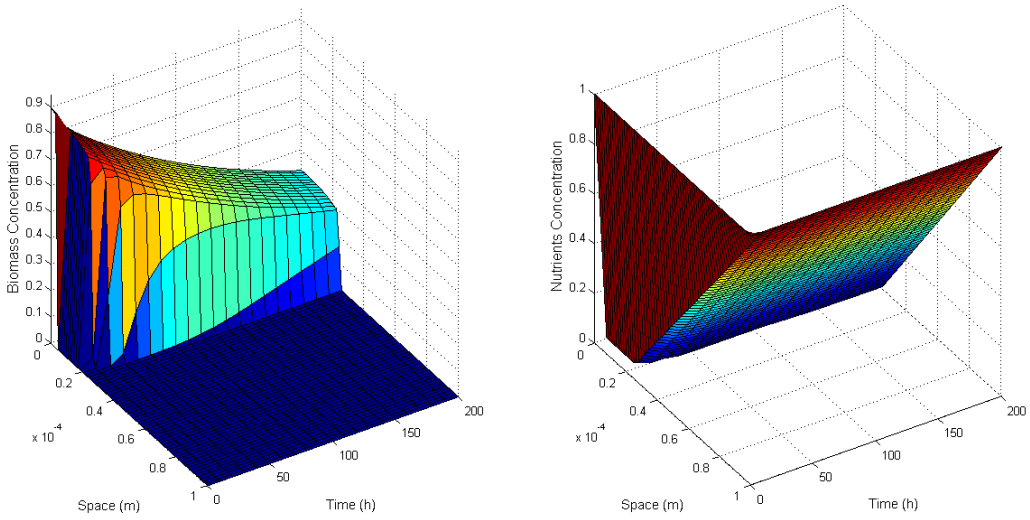

Figure 1: Case A: Biomass (left) and nutrients (right) concentrations at time $T = 200$ hours

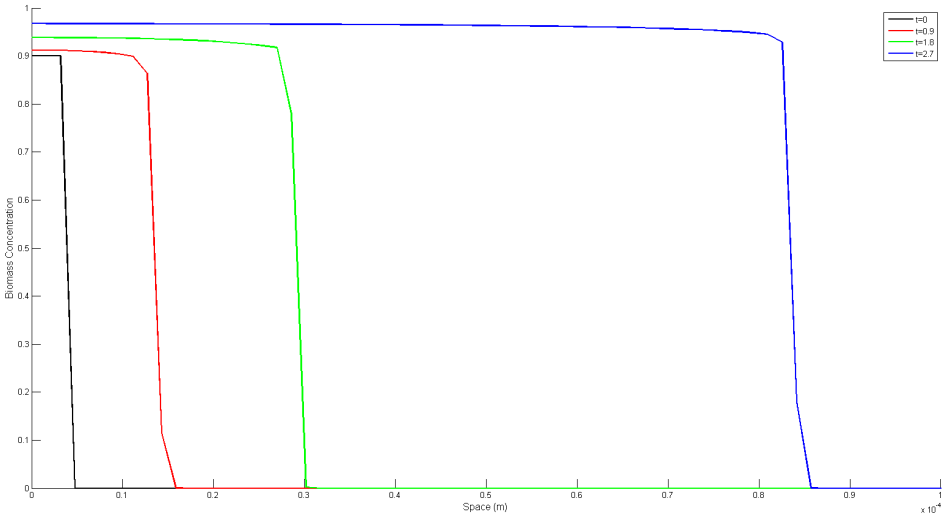

Figure 2: Case A: Evolution of biomass concentration with time

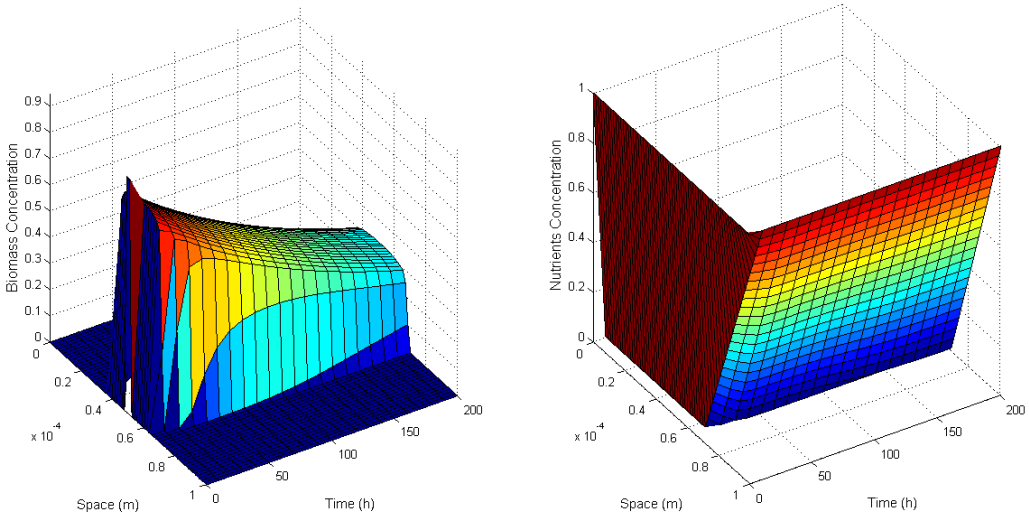

Figure 3: Case B-(a): Biomass (left) and nutrients (right) concentrations at time $T = 200$ hours

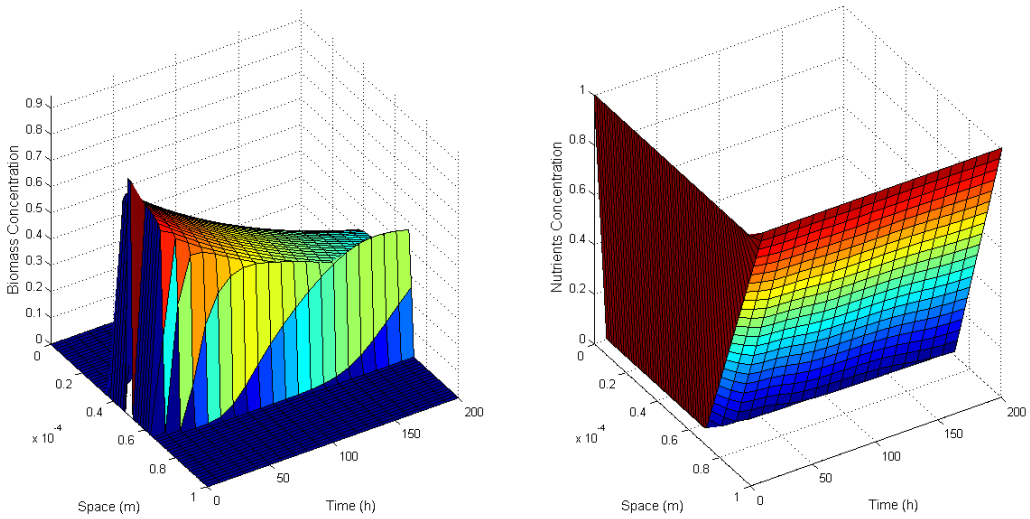

Figure 4: Case B-(b): Biomass (left) and nutrients (right) concentrations at time $T = 200$ hours

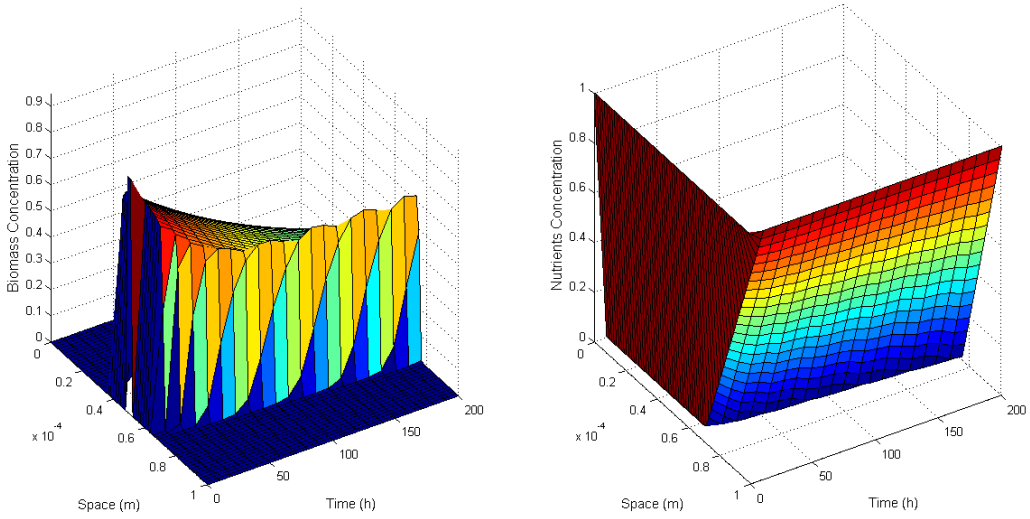

Figure 5: Case B-(c): Biomass (left) and nutrients (right) concentrations at time $T = 200$ hours

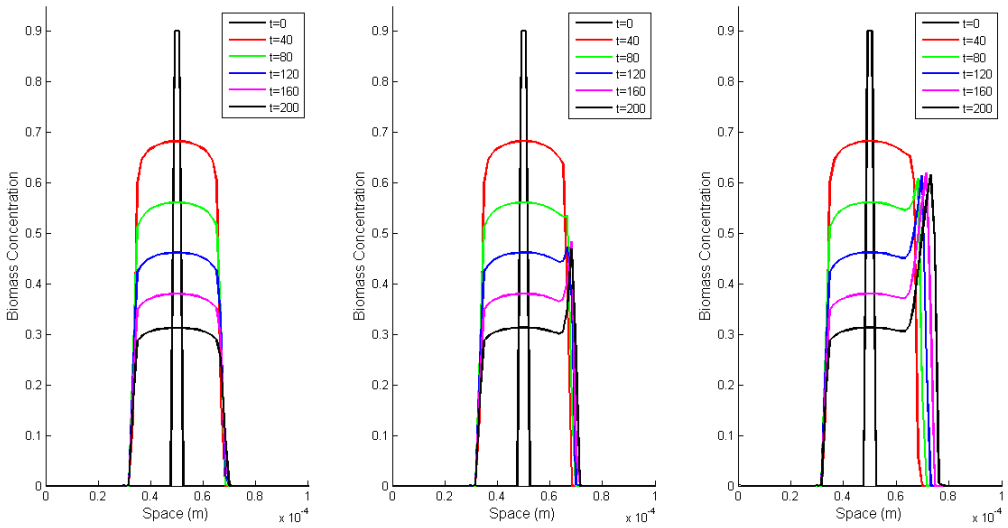

Figure 6: Evolution of biomass concentration with time in Cases B-(a) (left), B-(b) (center) and B-(c) (right)

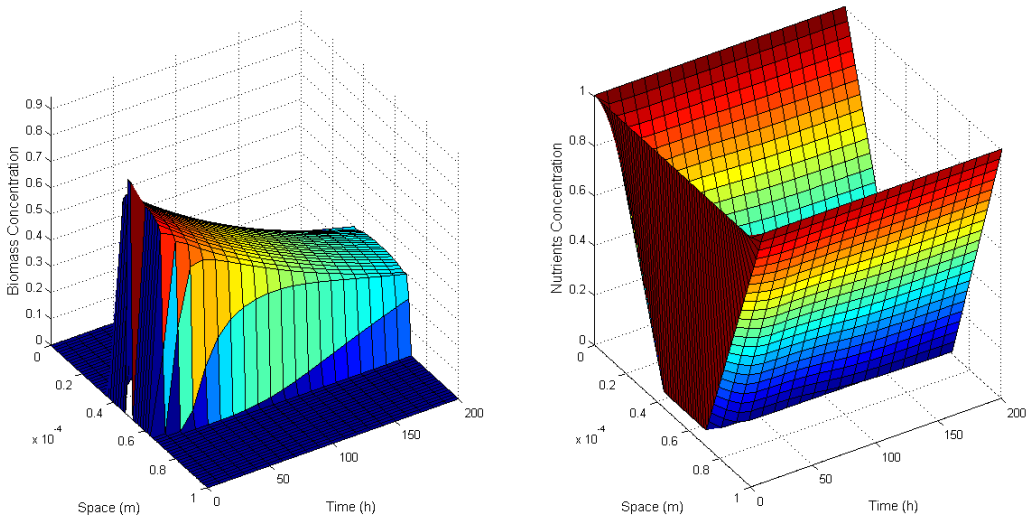

Figure 7: Case C: Biomass (left) and nutrients (right) concentrations at time $T = 200$ hours

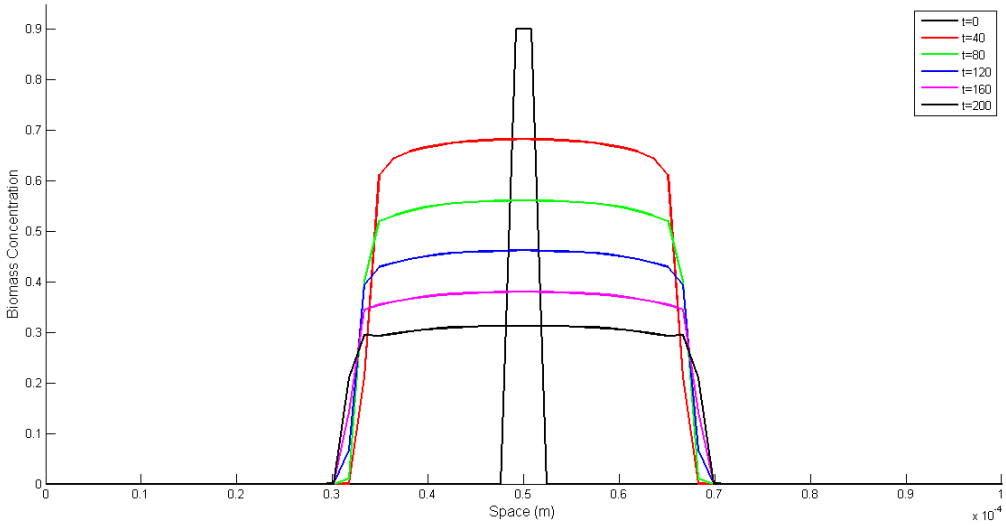

Figure 8: Case C: Evolution of biomass concentration with time

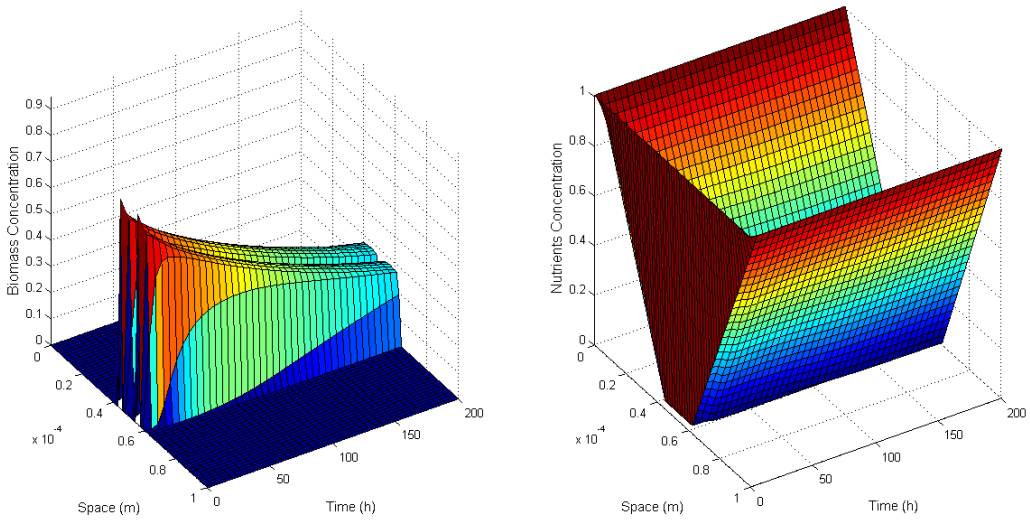

Figure 9: Case D-(a): Biomass (left) and nutrients (right) concentrations at time $T = 200$ hours

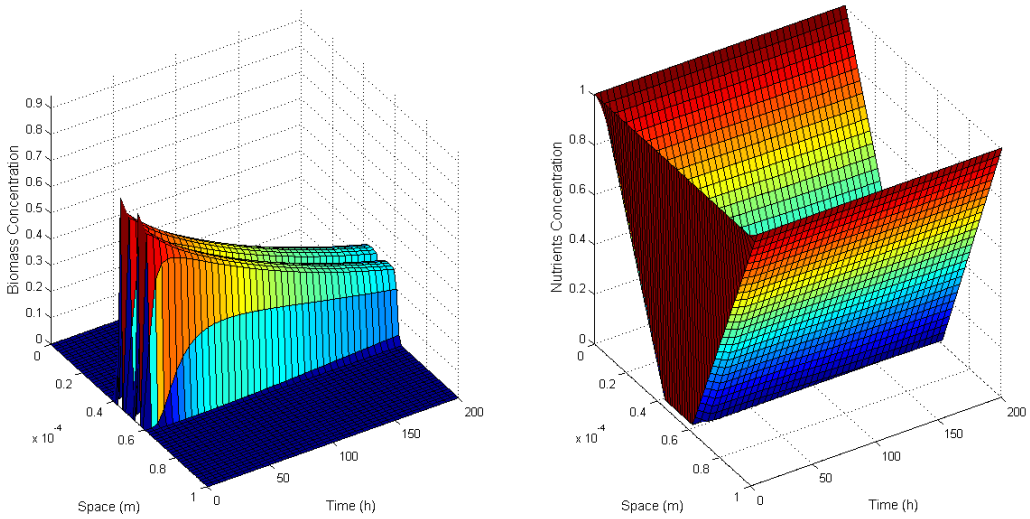

Figure 10: Case D-(b): Biomass (left) and nutrients (right) concentrations at time $T = 200$ hours

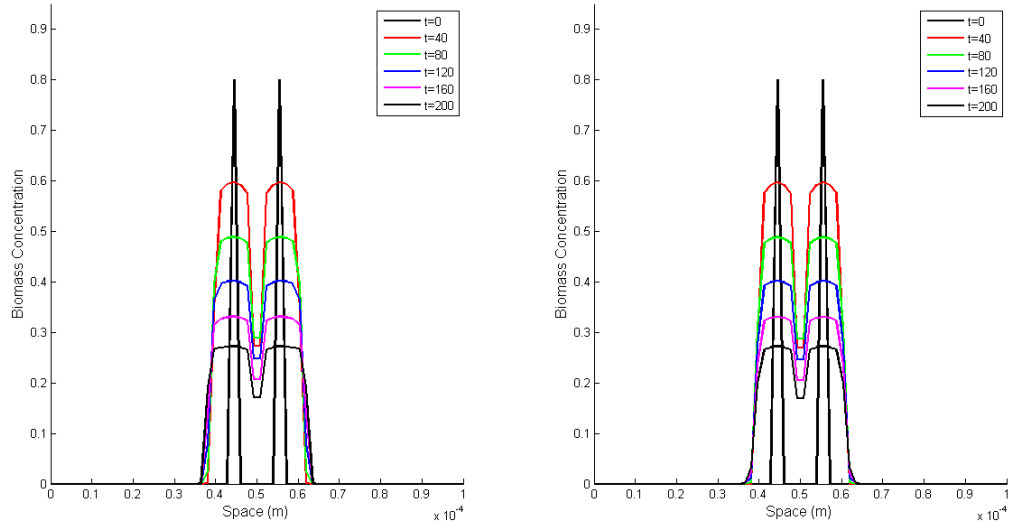

Figure 11: Evolution of biomass concentration with time in Cases D-(a) (left) and D-(b) (right)

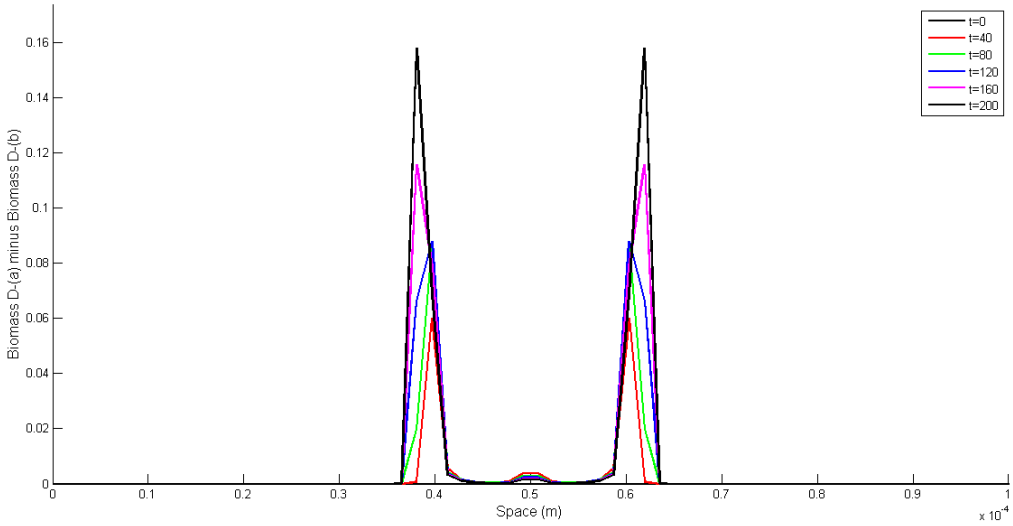

Figure 12: Case D: Biomass concentration in case D-(a) *minus* biomass concentration in Case D-(b) for different times

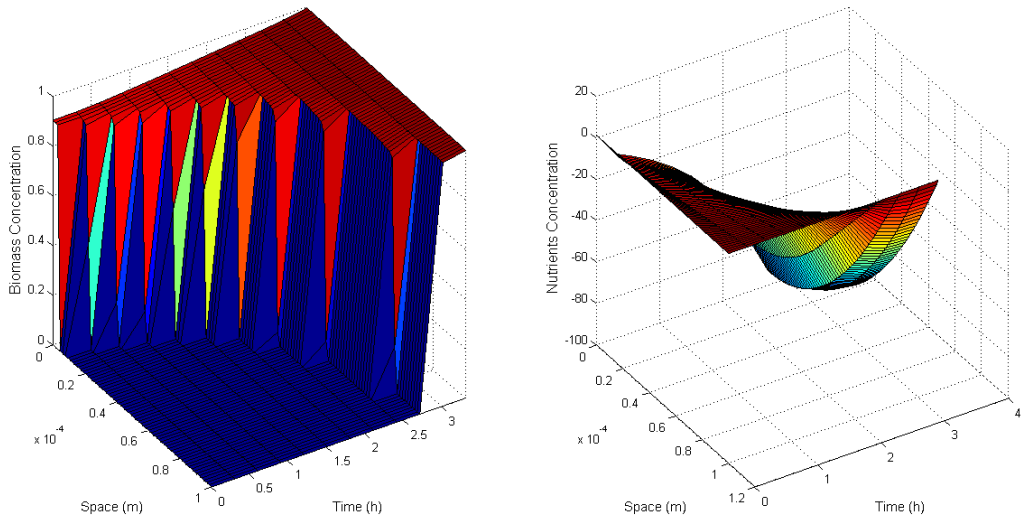

Figure 13: Case E-(a): Biomass (left) and nutrients (right) concentrations until time $T = T_0$ hours

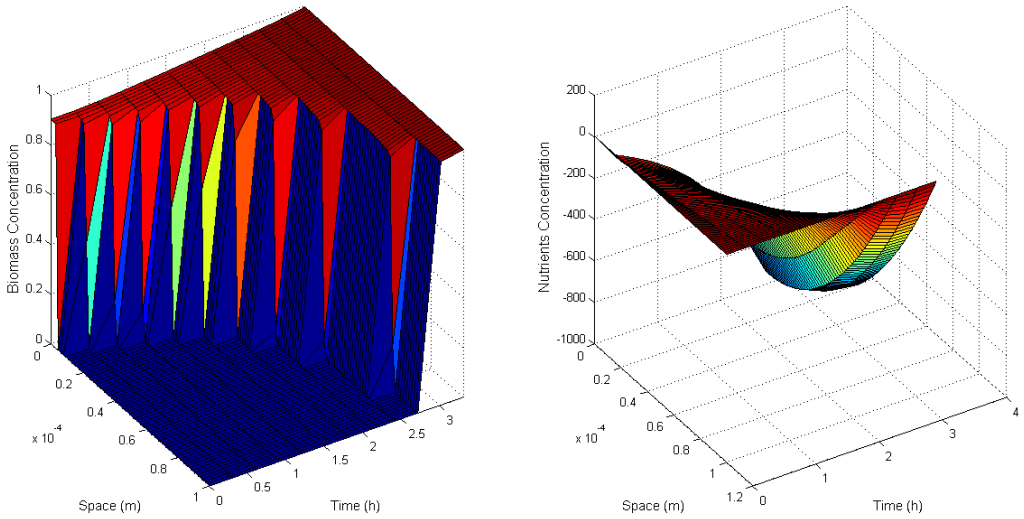

Figure 14: Case E-(b): Biomass (left) and nutrients (right) concentrations until time $T = T_0$ hours

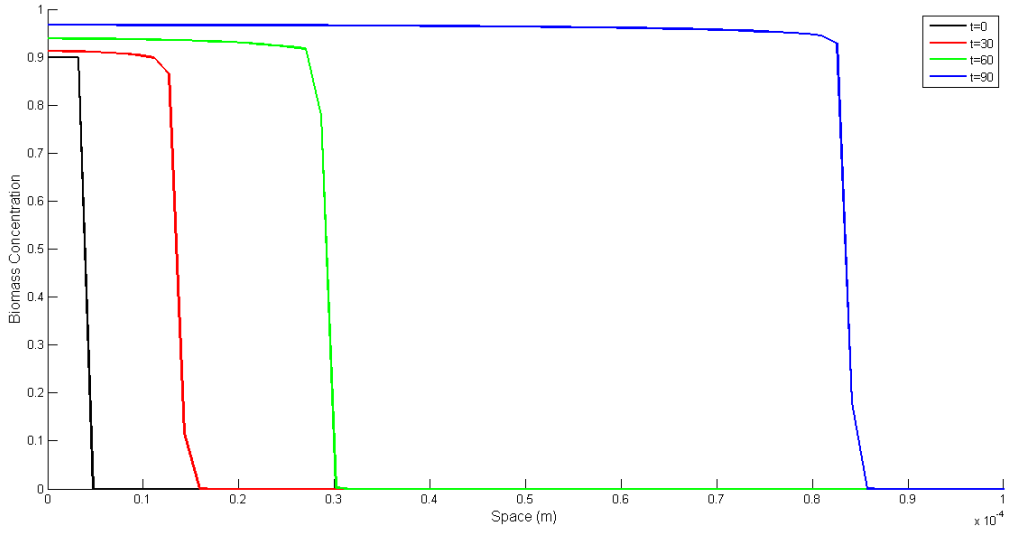

Figure 15: Case E-(a): Evolution of biomass concentration with time until blow up